

Numerical modeling and experimental considerations for a two-coil apparatus to measure the complex conductivity of superconducting films

Stefan J. Turneaure,^{a)} Aaron A. Pesetski, and Thomas R. Lemberger
*Department of Physics, The Ohio State University, 174 W. 18th Avenue, Columbus,
 Ohio 43210-1106*

(Received 1 December 1997; accepted for publication 9 January 1998)

We consider the accuracy of measurements of the complex conductivity of superconducting films with a two-coil mutual inductance technique. We present a numerical analysis of the procedure by which we deduce the real and imaginary parts of the conductivity, $\sigma = \sigma_1 - i\sigma_2$, of thin films from the in-phase and out-of-phase components of the mutual inductance of coaxial coils located on opposite sides of the film. The accuracy of the procedure is verified for the full ranges of film radii, thicknesses, and conductivities that are encountered for typical films of a wide variety of cuprate superconductors. We determine both experimentally and theoretically what effect flaws in the film would have on the accuracy of the measurement by examining the effects of holes located at various places in a superconducting film. The effect of capacitive coupling between the coils is measured and shown to be negligible when care is taken in grounding the drive and pickup coil circuits. The mutual inductance of the coils changes with temperature even with no sample present because the resistance of the coils changes and there is some thermal contraction. We describe a procedure for taking these effects into account. © 1998 American Institute of Physics. [S0021-8979(98)03108-9]

I. INTRODUCTION

The two-coil mutual inductance measurement is a simple nondestructive method for determining the conductivity of thin superconducting films. Since Fiory and Hebard¹ introduced the basic technique, a number of groups have used some variation of it to determine the sheet conductivity of thin films.²⁻⁸ The purpose of the present article is to detail our implementation and to estimate the uncertainty in the determination of σ_1 and σ_2 . A previous paper⁵ analyzed the case where σ is pure imaginary.

In our usual configuration, the primary (drive) and secondary (pickup) coils are located on opposite sides of the film. Many groups use this configuration and employ numerical procedures of varying degrees of complexity to extract the complex conductivity, $\sigma = \sigma_1 - i\sigma_2$, of the film from the measured complex mutual inductance, M . The basic procedure is to generate a “lookup” table consisting of values of M calculated for many different σ 's, and then to interpolate to get the σ that corresponds to a particular measured M . The difference among groups lies partly in the geometry of the coils and partly in the numerics of calculating the lookup table.

The literature provides several calculations of M as a function of σ for a general, homogeneous screen (film) placed between coils in various geometries.⁹⁻¹² We are interested in the case in which the coils are coaxial with each other and with a circular film, so that the geometry is azimuthally symmetric. A numerically tractable, exact solution exists for a film with arbitrary thickness and conductivity when the film radius is infinite,¹² but not for the usual experimental situation in which the radius of the film cannot be modeled accurately as infinite. For a film with a finite radius,

there is an exact solution only in the thin-film limit. In this article, we extend this solution to arbitrary thickness by using an *ad hoc* effective film thickness that is a function of the actual film thickness and conductivity.

Given that it is possible to calculate $M(\sigma_1, \sigma_2)$ for an arbitrary circular film, it would seem that the best procedure would be to calculate a lookup table that corresponds to the actual film radius and thickness and for the coil geometry used in the measurement. As discussed below, under certain circumstances, such as when the film radius is less than about five times the radius of the primary coil, this is the proper procedure to use. But sometimes a different procedure is preferred. For example, sometimes one would like to remove from the data the parasitic coupling between the primary and secondary coil circuits. Also, sometimes the sample film is square instead of circular and the direct calculation cannot be made. Under these circumstances, a better procedure is the one outlined in Refs. 5 and 8. One measures the mutual inductance at 4.2 K of, e.g., a 150 μm thick Pb foil of the same size and shape as the sample film, with nonconducting shims to keep the proper spacing between coils. Subtraction of this “zero position” mutual inductance from the mutual inductance measured with the real sample film present removes the parasitic coupling. As shown in Ref. 5 and in the present article to an excellent approximation it also removes the mutual inductance due to flux that “leaks around” the finite radius film but would not get through if the film had an infinite radius. The “corrected” mutual inductance data are normalized to the mutual inductance measured just above T_c to remove most of the uncertainty due to uncertainty in the coil geometry, such as coil spacing and diameter.⁵ Finally, assuming that the processed data are what would have been measured if the film radius had been infinite and the actual coils had been ideal circular, coaxial loops of wire, the lookup table is calculated from the

^{a)}Electronic mail: sjt@ohstpy.mps.ohio-state.edu

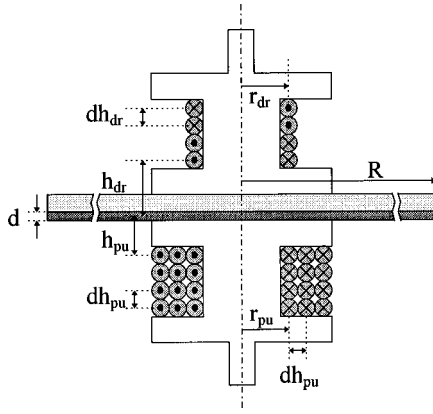


FIG. 1. The geometry of our two-coil apparatus (not to scale). The dots indicate current coming out of the page, and the crosses indicate current going into the page. The upper coil is the drive coil. There are actually 44 turns in the vertical direction in both the drive and pickup coils for our calculations.

exact expression for $M(\sigma_1, \sigma_2)$ for an infinite radius film with the same thickness as the sample.

In this article, we simulate the experimental subtraction procedure numerically for a particular coil geometry over all experimentally relevant conductivities and show that the results are in excellent agreement with the exact calculation for an infinite radius film as long as the film radius is at least five times larger than the coil radii. We discuss conditions where the direct calculation for a finite radius film is preferred on the basis of accuracy. However, it is worthwhile to note that there is a practical reason for using the subtraction procedure. It is very much faster to generate a lookup table for a film with infinite radius, which involves only a numerical integration than for a finite radius film, which involves numerical solution of an integral equation. The computation time to make a typical lookup table in the former case is roughly one minute; in the latter it is about one week.

The subtraction procedure is accurate for homogeneous films, but one is always worried that there may be a flaw in the substrate that propagates into a flaw in the film. Substrate flaws are typically small and rare. Still, one would like to know how sensitive the measurement is to them. Therefore, we present an experimental and numerical study of how holes in the film change the apparent conductivity. Finally we mention some sources of possible experimental error and how to eliminate them.

II. GEOMETRY

Figure 1 shows the geometry of the experiment. Circular loops of wire coaxial with each other and the film are located above and below the film, constituting the drive coil and pickup coil, respectively. Two important lengths are the radius of each loop and the distance of each loop from the film. The distance between the drive coil and the film is usually smaller than the coil radius, so the induced current density, $\mathbf{J}(\rho)$, in the film peaks at ρ equal to the radius of the coil. \mathbf{J} is proportional to the current, I_{dr} , in the drive coil. The currents in the film induced by each drive coil loop add linearly.

We define the complex mutual inductance as

$$M = M_1 + iM_2 = \frac{V_{pu}}{\omega I_{dr}}. \quad (1)$$

V_{pu} is the voltage across the pickup coil, i.e., the time derivative of the magnetic flux linking the pickup coil. Both the magnitudes and phases of I_{dr} and V_{pu} are measured. In the absence of a film, the phases of V_{pu} and I_{dr} are zeroed just above T_c so that the in-phase, inductive part of M, M_1 , is the bare mutual inductance of the coil assembly. We call the bare inductance the ‘‘initial position.’’ The out-of-phase, dissipative part of M, M_2 , comes entirely from dissipative currents associated with σ_1 in the film.

We use several different geometries for different measurements. Unless otherwise stated, data and calculations in this article pertain to the following representative geometry: $h_{dr} = 1.274$ mm; $h_{pu} = 0.271$ mm; and $r_{dr} = r_{pu} = 1.033$ mm. Note h_{dr} and h_{pu} are the distances from the center of the nearest loop of wire to the film for the drive and pickup coils, respectively. Both coils contain 44 turns in the vertical direction. The vertical length of the coil forms is 1.524 mm. The drive coil, containing one radial layer, has the upper 22 turns wound in the opposite direction from the lower 22 turns, as indicated in Fig. 1 by the dots and crosses. The pickup coil has 132 turns divided into three radial layers with all turns wound in the same direction. The separation between adjacent vertical loops and between radial layers is $dh_{dr} = dh_{pu} = 34.64$ μ m. The radius of the film is $R = 7.5$ mm, the thickness of the film is $d = 500$ \AA , and the frequency, $\omega/2\pi$, of the applied field is 50 kHz.

The above geometry is not necessarily the optimum geometry. Claassen *et al.* use thinner coils which are placed closer to the film,⁸ which leads to a greater sensitivity in $\Delta\lambda$. Lee *et al.* use an unequal number of turns wound in each direction of the drive coil to minimize the induced current density at the film boundary.⁶ This means that the magnetic field is parallel to the film edge, and that the flux leaking around the film is very small. It is very difficult to pin down the optimum coil arrangement. There are many things to consider such as how sensitive the results are to knowing the exact coil geometry, or to the presence of small holes in the film.

III. CALCULATION OF $M(\sigma_1, \sigma_2)$ FOR A FILM WITH INFINITE RADIUS

Following Clem and Coffey,¹² the solution for the mutual inductance between two coils separated by an infinite radius film of complex conductivity $\sigma = \sigma_1 - i\sigma_2$ and thickness d is given by

$$M(\lambda, \sigma_1, d) = \pi\mu_0 \frac{r_{dr}r_{pu}}{h} \times \int_0^\infty dx \frac{xe^{-x}}{x \cosh(\delta\chi) + \frac{\chi^2 + x^2}{2\chi} \sinh(\delta\chi)} \times J_1\left(x \frac{r_{dr}}{h}\right) J_1\left(x \frac{r_{pu}}{h}\right). \quad (2)$$

Here we assume only one loop for the drive coil and one loop for the pickup coil. The solution for multiple turn coils is just a superposition of the solution for single loops. Note h is the vertical separation between the drive and pickup loops minus the film thickness, d . The drive coil and pickup coil radii are labeled r_{dr} and r_{pu} , respectively. In Eq. (2), $\delta \equiv d/h$ and $\chi^2 \equiv x^2 + (h/\lambda)^2 + i\mu_0\omega\sigma_1 h^2$, and σ_2 is related to the magnetic penetration depth, λ , through the relation $\sigma_2 = 1/\mu_0\omega\lambda^2$. J_1 is a cylindrical Bessel function. The prefactor is μ_0 times the geometric mean of the areas of the drive and pickup loops divided by the distance h between the loops. For a typical geometry, it is roughly equal to the mutual inductance when the currents in the film are negligible.

We consider the limit where the spacing, h , between coils is much larger than λ , which is the usual situation. The integrand in Eq. (2) is cut off at large x because of the “ e^{-x} ” factor. Numerical calculations show that integrating to $x=20$ guarantees high accuracy for essentially any coil geometry, with the largest part of the integral coming from $x < 5$. Since $h \gg \lambda$, the real part of χ^2 is much greater than x^2 for the significant region of integration, and $\chi^2 + x^2 \approx \chi^2 \approx (h/\lambda)^2 + i\mu_0\omega\sigma_1 h^2 = i\mu_0\omega\sigma h^2$. Under these conditions, taking the thin-film limit, $d \rightarrow 0$, Eq. (2) reduces to

$$M(\lambda, \sigma_1, d \rightarrow 0) = \pi\mu_0 \frac{r_{\text{dr}}r_{\text{pu}}}{h} \int_0^\infty dx \frac{xe^{-x}}{x + \frac{i\mu_0\omega h\sigma}{2}} d \times J_1\left(x \frac{r_{\text{dr}}}{h}\right) J_1\left(x \frac{r_{\text{pu}}}{h}\right) \text{ [thin-film limit]}. \quad (3)$$

This result can also be obtained by using the method of Jeanneret *et al.*,² who considered the geometry where a dipolar drive coil and a quadrupolar pickup coil reside on the same side of the film. They treated the film as having zero thickness and a sheet conductivity, σd .

The purpose in deriving Eq. (3) is to obtain an expression for an effective film thickness, $d_{\text{eff}}(d, \sigma)$ that is a function of the actual film thickness, d , and conductivity, σ , such that when “ d ” in the thin-film expression, Eq. (3), is replaced by $d_{\text{eff}}(d, \sigma)$, Eq. (3) gives a mutual inductance that is very close to the exact result, from Eq. (2). To guide our choice, we rewrite Eq. (2) with the approximation $h \gg \lambda$, but without taking the thin-film limit:

$$M \approx \pi\mu_0 \frac{r_{\text{dr}}r_{\text{pu}}}{h} \int_0^\infty dx \times \frac{xe^{-x}}{x \cosh(d\sqrt{i\mu_0\omega\sigma}) + \frac{i\mu_0\omega\sigma h}{2} \frac{\sinh(d\sqrt{i\mu_0\omega\sigma})}{\sqrt{i\mu_0\omega\sigma}}} \times J_1\left(x \frac{r_{\text{dr}}}{h}\right) J_1\left(x \frac{r_{\text{pu}}}{h}\right). \quad (4)$$

It is not obvious how to approximate Eq. (4) by defining an effective thickness because “ d ” appears in two different places in the denominator of Eq. (4) and only one place in Eq. (3). However, it turns out that the “ $\cosh[d(i\mu_0\omega\sigma)^{1/2}]$ ”

in the denominator can be set equal to unity even when it is not, i.e., when d is much larger than the complex “skin depth,” $(i\mu_0\omega\sigma)^{-1/2}$. The reason is that when this term is large the “sinh” term in the denominator is much larger because the spacing between coils, h , is always very much larger than $(\mu_0\omega\sigma)^{-1/2}$. With this in mind, comparison of Eq. (4) with Eq. (3) leads to the identification:

$$d_{\text{eff}}(d, \omega\sigma) = \frac{\sinh(d\sqrt{i\mu_0\omega\sigma})}{\sqrt{i\mu_0\omega\sigma}}. \quad (5)$$

Note that d_{eff} is a complex function of d and of $\omega\sigma$. When the film impedance is purely inductive, $\sigma = -i\sigma_2$, this expression reduces to the result, $d_{\text{eff}} \approx \lambda \sinh(d/\lambda)$. In the thin-film limit, $d \ll \lambda$, we recover $d_{\text{eff}} \rightarrow d$. In the opposite limit, $d_{\text{eff}} \approx \lambda e^{d/\lambda}$. This is because a thick film attenuates the mutual inductance exponentially with film thickness, rather than as “ $1/d$.” The final justification of this choice for d_{eff} is that M calculated from the exact expression, Eq. (2), and from the thin-film expression, Eq. (3), with d replaced by d_{eff} agree within a fraction of a percent for all reasonable values of σ .

To make contact with a method used by Claassen *et al.*⁸ to determine λ , we obtain the limiting case of Eq. (4) when $\sigma_1 \ll \sigma_2$. This is the usual case, except for temperatures within a degree or so of T_c . In this case, $\chi \approx h/\lambda$, and for $\lambda^2 \ll hd$ the denominator reduces to $(h/2\lambda)\sinh(d/\lambda)$. Equation (4) may be written as

$$M(\lambda, \sigma_1 \ll \sigma_2, d) \approx \frac{\lambda}{\sinh\left(\frac{d}{\lambda}\right)} \left[2\pi\mu_0 \frac{r_{\text{dr}}r_{\text{pu}}}{h^2} \int_0^\infty dx x e^{-x} \times J_1\left(x \frac{r_{\text{dr}}}{h}\right) J_1\left(x \frac{r_{\text{pu}}}{h}\right) \right]. \quad (6)$$

This is the expression Claassen *et al.*⁸ use to determine λ .

IV. CALCULATION OF $M(\sigma_1, \sigma_2)$ FOR A FINITE RADIUS FILM

We derive an integral equation for the sheet current density in a finite radius film in the thin-film limit, then insert $d_{\text{eff}}(d, \omega\sigma)$ in place of “ d ” in the equation to extrapolate to thick films. Since the derivation was presented in Ref. 5, here we just outline the method pointing out improvements and the changes which have been made to accommodate a non-zero σ_1 .

The full integral equation to be solved for the current density, $\mathbf{J}(\mathbf{r})$, in the film is

$$\mathbf{A}_{\text{dr}}(\mathbf{r}) = \frac{\mathbf{J}(\mathbf{r})d}{-i\omega\mu_0\sigma d} - \frac{\mu_0}{4\pi} \int d^3r' \frac{\mathbf{J}(\mathbf{r}')}{|\mathbf{r} - \mathbf{r}'|}, \quad (7)$$

where $\mathbf{A}_{\text{dr}}(\mathbf{r})$ is the vector potential in the film due to the drive currents and $\mathbf{J}(\mathbf{r})$ is the current density in the film. Both $\mathbf{A}_{\text{dr}}(\mathbf{r})$ and $\mathbf{J}(\mathbf{r})$ are azimuthally symmetric. Note σ could be a function of the radial coordinate, a fact that we will use to simulate holes in the film. For a thin film, $\mathbf{J}(\mathbf{r})$ is essentially uniform through the thickness, and the integral over z results in multiplication by d . The integral over the azimuthal angle, ϕ , is done analytically. We are left with a one-dimensional integration over the radial coordinate ρ . This integral is

changed into a discrete sum by partitioning the film into N annular rings centered at radii, r_i , with widths Δr_i . The integral equation is thus converted into an $N \times N$ matrix equation with the unknown vector being the sheet current in the i th ring, K_i . Once the K_i have been determined, calculation of M is straightforward.

The matrix elements in the discrete representation of the integral are simply related to the mutual inductance between rings. There are a variety of ways to calculate the mutual inductance between rings. Calculation of the self-inductance of a ring is complicated because the integral kernel contains a logarithmic singularity. Gilchrist and Brandt discuss the calculation of matrix elements in detail in Ref. 9. They show that a sum rule must be obeyed for the elements of the mutual inductance matrix, and that there is an analytic form for the self-inductance of a ring (for $r_i \gg \Delta r_i$) which very closely satisfies the sum rule. The exact analytic form depends on how the off-diagonal matrix elements are calculated. For the mutual inductance between different rings we treat the rings as thin wires located at the center of the rings. With this choice for the off-diagonal matrix elements, Gilchrist and Brandt⁹ have shown that the proper self-inductance of a ring for the sum rule to be satisfied is given by

$$M_{ii} = \mu_0 r_i \left(\ln \left[\frac{8 \pi r_i}{\Delta r_i / 2} \right] - 2 \right). \quad (8)$$

Using Eq. (8) for the self-inductance yields a rapid convergence for the mutual inductance with increasing matrix size. Very high accuracy is obtained for as few as $N=100$ rings. This is an improvement over Ref. 5, where we used a different method to calculate the diagonal matrix elements. To obtain accurate results we were forced to do the calculation several times with different numbers of rings and then to extrapolate to the limit of an infinite number of rings.

V. SUBTRACTION AND NORMALIZATION PROCEDURE

In this section we explore the procedure by which the measured complex mutual inductance is converted to a complex conductivity. Various quantities come into play. $M_E(\lambda, \sigma_1, d, R)$ is the experimental mutual inductance for a film with radius R and thickness d , measured at angular frequency ω . In the numerical simulation, it is denoted $M_F(\lambda, \sigma_1, d_{\text{eff}}, R)$, and calculated for a film with radius R by using the finite radius, thin-film expression, Eq. (7), with d replaced by $d_{\text{eff}}(d, \omega \sigma)$. In the lab, we subtract from $M_E(\lambda, \sigma_1, d, R)$ the mutual inductance $M_E(\lambda \ll d, 0, d, R)$ measured with a placebo (Pb) foil in place of the sample film. We refer to this mutual inductance as the *zero position*, $M_E(0, 0)$, since it is the coupling when there is zero coupling “through” the sample. The assumption is that subtraction of the coupling that goes “around” the film leaves only the coupling that would have gone “through” the film if it had infinite radius. Experimentally, the subtraction has the additional advantage that it removes stray coupling between the drive and pickup coils. To simulate the experimental subtraction, we subtract $M_F(\lambda \ll d, \sigma_1 = 0, d_{\text{eff}}, R)$ from $M_F(\lambda, \sigma_1, d_{\text{eff}}, R)$. The experimental “data,” corrected for

the finite radius of the film, are compared with the exact mutual inductance, $M_I(\lambda, \sigma_1, d)$, calculated for a film with infinite radius and thickness d by numerical integration of Eq. (2). We will see that under a very large range of parameters, the “data” and the infinite-radius film calculation agree within a fraction of a percent justifying both the subtraction procedure and the use of effective thickness.

In the lab, it is useful to do an additional step that is not necessary in the numerical simulation. That step is to normalize the “corrected” data to the mutual inductance measured just above the T_c , where the film response is negligible. For typical coils, a 1000 Å thick film produces a detectable signal when $|\sigma|$ exceeds about $1 (\mu\Omega \text{ cm})^{-1}$. The normalization removes uncertainties associated with amplifier gains and the exact geometry of the coils. The mutual inductance measured when there is no screening ($\sigma \approx 0$) is called the *initial position*, labeled $M(\infty, 0)$. Since the film response is negligible, $M(\infty, 0)$ is independent of the film radius and thickness. For both the *zero position* and the *initial position*, $M_2 = 0$. To summarize, from our data we calculate

$$\frac{M_E(\lambda, \sigma_1, d, R) - M_E(0, 0)}{M_E(\infty, 0)}, \quad (9)$$

then find λ and σ_1 by using a lookup table containing the normalized real and imaginary mutual inductances, $M_{I,1}(\lambda, \sigma_1, d) / M_f(\infty, 0)$ and $M_{I,2}(\lambda, \sigma_1, d) / M_1(\infty, 0)$, calculated for an infinite radius film and for coils that are as close as possible to the actual coils in the probe. The following numerical simulation of the procedure argues that it works well.

VI. COMPARISON BETWEEN FINITE RADIUS AND INFINITE RADIUS FILM SOLUTIONS

We now show that our analysis procedure is accurate for conductivities which cover the relevant regions encountered in experiment. Figure 2 shows values of σ_1 and σ_2 typically encountered at a measurement frequency of 50 kHz upon cooling a film of YBCO from a few degrees above T_c to the lowest temperatures. We define three temperature regions. Over the highest half Kelvin or so when the film response is first detectable, σ_1 and σ_2 are roughly equal, and they both grow as T decreases. Note σ_1 reaches a peak at a temperature which is sometimes defined as T_c . In the next Kelvin or two, σ_1 decreases from its peak value while σ_2 continues to increase. Eventually, σ_1 gets to be so much less than σ_2 that the uncertainty of a fraction of a degree in the absolute phase of the measured mutual inductance means that the film response is purely inductive, within experimental uncertainty. At 50 kHz the peak value of σ_1 is never observed to be greater than $10^{11} (\Omega \text{ m})^{-1}$ for YBCO. For comparison with Fig. 2, Fig. 3 shows the conductivity for a 3% cobalt-doped YBCO film. Figures 2 and 3 establish the conductivities that are typical in the lab.

To compare the numerically generated “corrected data” for a film with conductivity σ , thickness d , and radius R to the mutual inductance calculated for a film with the same σ and d but an infinite radius, we define the differences in

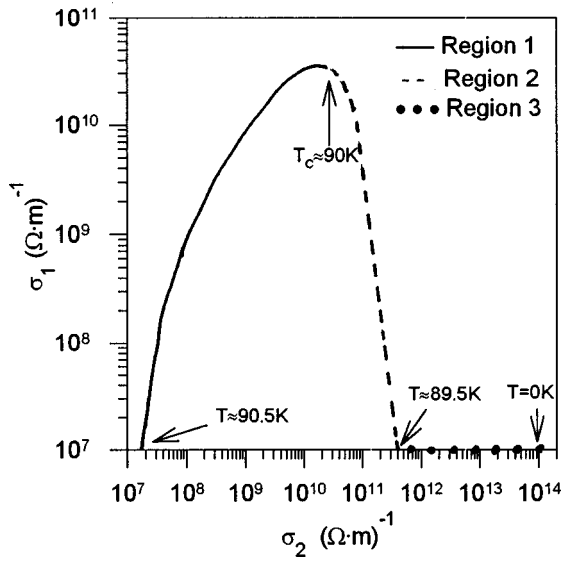


FIG. 2. A schematic drawing of the conductivities observed for high T_C superconducting films from the two coil mutual inductance technique at 50 kHz. In region 3, σ_1 is less than $10^7 (\Omega \cdot m)^{-1}$ and is too small to measure.

the real and imaginary mutual inductances: $\Delta M_1 \equiv [M_{F,1}(\lambda, \sigma_1, d_{\text{eff}}, R) - M_{F,1}(\lambda \ll d, 0, d_{\text{eff}}, R) - M_{I,1}(\lambda, \sigma_1, d)]$ and $\Delta M_2 \equiv [M_{F,2}(\lambda, \sigma_1, d_{\text{eff}}) - M_{I,2}(\lambda, \sigma_1, d)]$. We will see that the percent differences, $P_{M1} \equiv 100\Delta M_1 / M_{I,1}$ and $P_{M2} \equiv 100\Delta M_2 / M_{I,2}$, are small for all relevant complex conductivities by exploring three regimes. The first regime is $\sigma_1 \ll \sigma_2$, which corresponds to the low temperature region 3 of Fig. 2. Since this region was discussed in detail in Ref. 5, we just mention that $|P_{M1}|$ is less than 0.08 for $\lambda > 200 \text{ \AA}$. To put this into concrete terms, it means that the subtraction procedure for data analysis results in a 1 \AA error in λ for a film with $\lambda = 1500 \text{ \AA}$, $d = 1000 \text{ \AA}$, and $R = 7.5 \text{ mm}$. This is negligible compared with that from the uncertainty in the film thickness.

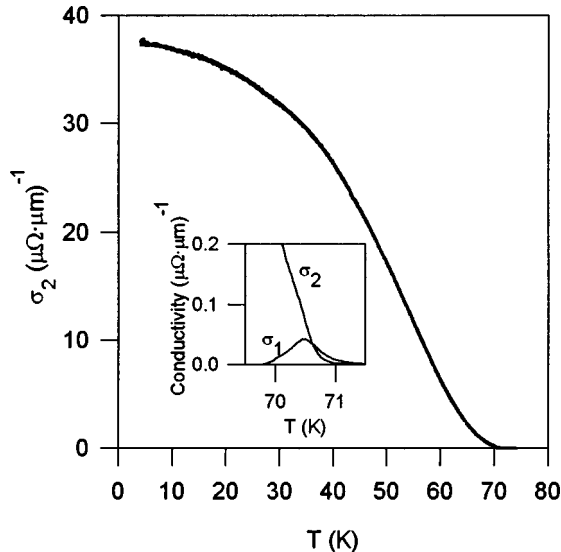


FIG. 3. An example of the experimentally determined complex conductivity for a 3% Co-doped YBCO thin film. The inset shows both the real and imaginary parts of the conductivity near the transition temperature.

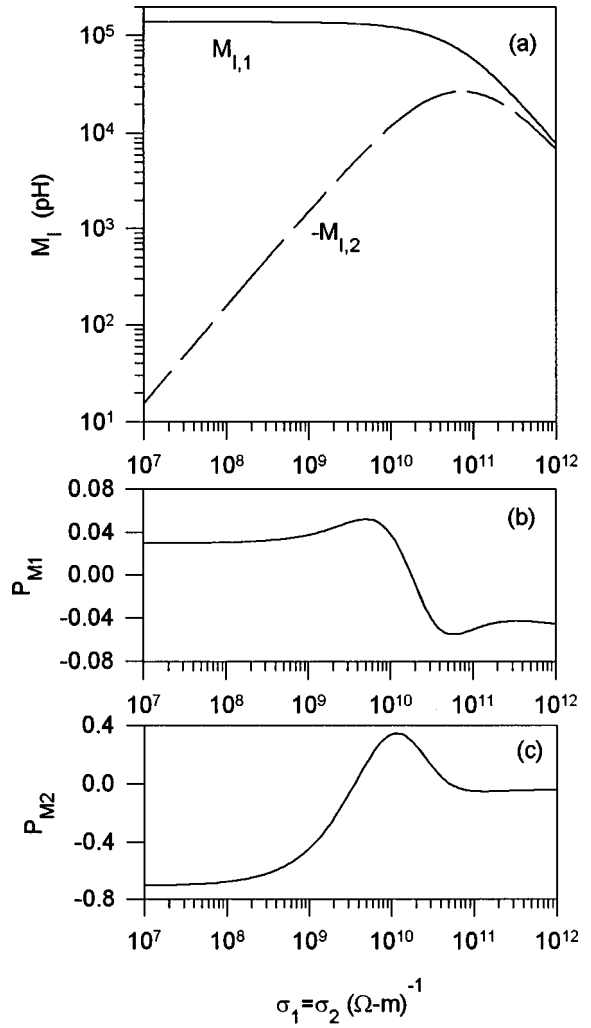


FIG. 4. (a) Mutual inductance, M , calculated for an infinite area film with $\sigma_1 = \sigma_2$. The geometry of the coils is described in the text. The percent differences between M calculated for an infinite area film and for a finite area film using the subtraction procedure are shown as (b) $P_{M1} = 100^* [M_{F,1} - M_F(\lambda = 0, \sigma = 0) - M_{I,1}] / M_{I,1}$ and (c) $P_{M2} = [M_{F,2} - M_{I,2}] / M_{I,2}$.

The second regime is $\sigma_1 = \sigma_2$, which corresponds to the high temperature region 1 in Fig. 2. Figure 4 shows P_{M1} and P_{M2} as functions of σ_1 over the relevant range of σ_1 . The real and imaginary inductances, $M_{I,1}$ and $-M_{I,2}$, calculated for an infinite radius film are shown for scale. Note that $M_{I,2}$ is the “dissipative” coupling coming from σ_1 , so it is proportional to σ_1 for small σ . In any case, $|P_{M1}|$ is always less than 0.08, and $|P_{M2}|$ is less than 0.8. Both of these errors are negligible. As discussed below, for conductivities below the crossover where P_{M1} and P_{M2} have local maxima, it is more accurate to model the experiment directly rather than to do the subtraction. This becomes more important when the radius of the film is less than about five times the radius of the coils.

The third regime corresponds to the narrow intermediate temperature range just below “ T_C ,” region 2 in Fig. 2. For ten values of σ_2 , corresponding to λ 's from $1 \mu\text{m}$ to 1 mm , we calculated P_{M1} and P_{M2} for several values of σ_1 between 10^7 and $10^{12} (\Omega \cdot m)^{-1}$. (For λ 's shorter than $1 \mu\text{m}$, the val-

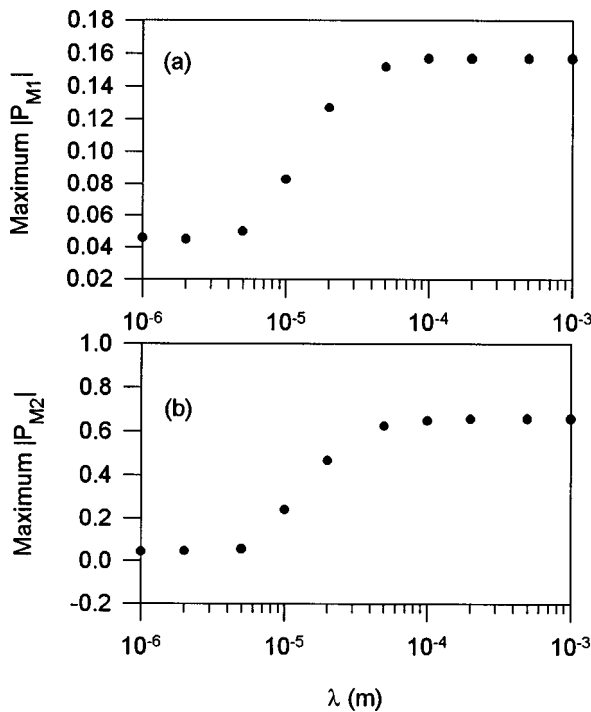


FIG. 5. Worst case percent differences between infinite area and finite area film calculations using the subtraction procedure as a function of the penetration depth, where real conductivities between 10^7 and $10^{12} (\Omega \text{ m})^{-1}$ were tested for each penetration depth. (a) $P_{M1} = 100 * [M_{F,1} - M_F(\lambda = 0, \sigma_1 = 0) - M_{I,1}] / M_{I,1}$ and (b) $P_{M2} = [M_{F,2} - M_{I,2}] / M_{I,2}$.

ues of σ_1 observed in the experiment are negligible compared with σ_2 and the measured M_2 cannot be differentiated from zero.) For each value of λ , we determined the largest values of the percent differences, $|P_{M1}|$ and $|P_{M2}|$, that were encountered as σ_1 varied. These maximum values, plotted in Fig. 5 vs λ , are so small that it doesn't matter what value of σ_1 they correspond to. In all cases, the error is smaller than the errors arising from uncertainties in the coil geometry and film thickness.

As mentioned above, if the radius of the film is less than about five times the radii of the coils, it is more accurate to skip the subtraction procedure and use the finite-radius film calculation directly to create the lookup table. The reason that the subtraction procedure breaks down at low conductivities is the following. As long as the "skin depth" is much smaller than a geometric factor such as $(hd)^{1/2}$, the current density at points 4 mm or more away from the center of an infinite radius film would be nearly zero. However, as σ decreases and the skin depth increases the current distribution spreads out further from the center of the film. At low enough conductivities the current distribution is simply proportional to the applied field. Figure 6 shows the current density as a function of the radial coordinate for $\sigma_1 = \sigma_2$. The current densities, J_1 (in-phase with the drive current), and J_2 (out-of-phase with the drive current) are normalized to their peak values below the drive coil radius. The solid line is for a finite radius film and the dashed line is for an infinite radius film. As the conductivity is increased from zero the normalized current density changes from the low conductivity limiting form shown for $\sigma_1 = 10^7 (\Omega \text{ m})^{-1}$ up

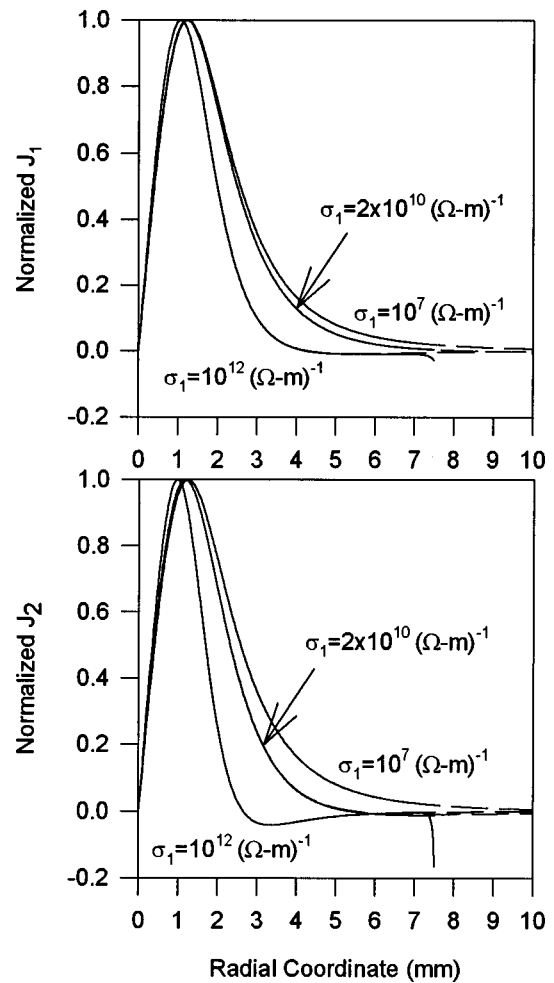


FIG. 6. Current density for $\sigma_1 = \sigma_2$ normalized to the peak value below the drive coil for a 7.5 mm radius film. The solid lines are for a finite radius film and the dashed lines are for an infinite radius film. J_1 and J_2 are respectively in-phase and out-of-phase with the drive current. There is a range of conductivities in which the normalized current densities crosses over from the form for $\sigma_1 = 10^7 (\Omega \text{ m})^{-1}$ to the form for $\sigma_1 = 10^{12} (\Omega \text{ m})^{-1}$.

to the high conductivity limiting form shown for $\sigma_1 = 10^{12} (\Omega \text{ m})^{-1}$. The change in shape of the normalized current density occurs over a range in which σ increases by about a factor of 100. At low conductivities a significant fraction of the current density is located beyond 5 mm from the center of the film. The reason that $|P_{M2}|$ is larger than $|P_{M1}|$ is that, in contrast to the "inductive" coupling M_1 , the "dissipative" coupling, M_2 , results only from dissipative currents, J_2 , associated with σ_1 in the film. When σ gets large enough that a significant fraction of the in-phase current is beyond 5 mm from the center of the film the screening is very weak such that M_1 is dominated by the current in the drive coil. In Fig. 4, the departure of P_{M2} from zero for $\sigma_1 = \sigma_2 < 10^{10} (\Omega \text{ m})^{-1}$ is dominated by this finite film effect.

It is worth returning to the question of the accuracy of extending the finite-radius, thin-film expression to arbitrary film thicknesses. Based on the excellent agreement found just above, we conclude that the error is negligible for 500 Å thick films. The percent differences between M calculated from Eq. (2) and from Eq. (3) using the effective thickness are about 10^4 times smaller than P_{M1} and P_{M2} presented in

Figs. 4 and 5. Thus it is reasonable to assume that P_{M1} and P_{M2} are dominated by finite radius effects and not by the use of the effective thickness. We have done the same calculations as presented in Figs. 4 and 5 for films with d ranging from 30 Å to 1 μm and find that the maximum P_{M1} 's and P_{M2} 's resulting from the subtraction procedure are nearly identical to their maximum values when the film is 500 Å thick, although they occur at different values of σ . An alternate, though in our opinion unlikely, view would be that the error in the subtraction procedure is exactly compensated by the error in the thin-film effective thickness approximation.

We have checked the subtraction procedure for other coil geometries such as that used by Claassen *et al.*⁸ For a dipolar drive coil and a dipolar pickup coil, $|P_{M1}|$ and $|P_{M2}|$ are roughly four times larger than for the quadrupolar drive coil and dipolar pickup coil used in the calculations presented above. For a 7.5 mm radius film, the error is still much smaller than the uncertainty in λ due to uncertainty in the film thickness.

VII. EXPERIMENTAL CONSIDERATIONS

There are some technical details that were left out of the discussion in the previous section. As the sample is cooled, some thermal contraction occurs and the resistance, $R_{pu}(T)$, of the pickup coil decreases. As the pickup coil impedance changes, the effective gain and phase shift of the preamplifier used to amplify V_{pu} change. The gain changes by a few percent and the phase changes by a few degrees, typically. These must be compensated for. Small errors in the phase of V_{pu} will lead to large errors in σ_1 when σ_2 is large. The accuracy of σ_1 just below T_C depends critically on how well the phase of V_{pu} is known. The inset of Fig. 3 shows the peak in σ_1 , for reference.

We introduce $M_B(T)$, the background mutual inductance, which is the mutual inductance measured with a filmless substrate (nonconducting) inserted between the coils. The normalized background, $M_B(T)/M_B(T_0)$, is a measure of the T dependence of the effective gain and phase shift of our amplifiers as well as of thermal contractions. Below 30 K, $M_B(T)$ is nearly independent of T . To correct the experimental data for the temperature dependent gain and phase shift we use the following quantity instead of that given by Exp. (9) to determine the normalized mutual inductance which is to be inverted to find λ and σ_1 :

$$\frac{M_E(\lambda, \sigma_1, T)/M_E(\infty, 0, T_0)}{M_B(T)/M_B(T_0)} = \frac{M_E(0, 0, 4K)}{M_E(\infty, 0, 4K)}. \quad (10)$$

In the experiment, the phases of M_E and M_B are zeroed at T_0 , where T_0 is a few K higher than T_C . $M_E(0, 0, 4K)$ is measured with a 150 μm thick Pb foil of the same size and shape as the film to be measured. $M_E(\infty, 0, 4K)$ is then measured by replacing the Pb foil by a 150 μm thick glass slide. For the measurement of M_B , shims separate the coils so that $M_B(T_0)$ is very close to $M_E(\infty, 0, T_0)$.

Another temperature dependent effect is that the skin effect changes the current distribution within the wires of the coils as the conductivity of the wires changes, forcing the currents to reside in a thin sheath at the surface of the wire at

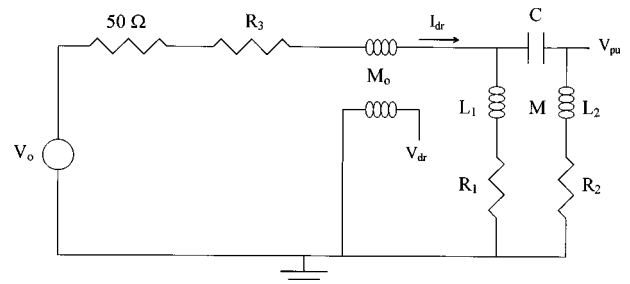


FIG. 7. Model circuit of the experiment. The drive current is measured through the mutual inductor M_0 . The capacitor C represents the very small capacitance between the drive and pickup coils. If either R_1 or R_2 is not small, leakage current through the capacitor causes an additional voltage in the measured V_{pu} which becomes significant as M get small.

low T . This physically changes the bare mutual inductance, M_B . This problem is minimized by using very fine wire (roughly 25 μm diameter). Any remaining effect is diminished by the procedure in Exp. (10). Another advantage to using fine wire is that more turns can be made in close proximity to one another so that the current is almost a continuous sheet and the normalized mutual inductance is less sensitive to any imperfections in the coil windings.

The mutual inductance as normalized in Exp. (10) should have a phase of zero at low temperatures, where $\sigma_1 \ll \sigma_2$. In practice the phase is usually less than 1°. However if the circuit is not grounded properly, capacitive coupling between the drive and pickup coils can lead to a large spurious phase for M . Figure 7 shows a model of the experimental circuit that includes the capacitive coupling as a lumped circuit element. The single capacitor, C , effectively represents the net capacitance between the wires in the drive and pickup coils. If either the drive or pickup coil circuit has a high impedance to ground, then when the mutual inductance, M , becomes small due to screening by a film the measured value of M will be incorrect. This is because some of the current, $|I_{dr}| = |V_{dr}|/(\omega M_0)$, will go to ground through the capacitor and develop an extra voltage across the pickup coil. Even a very small leakage current can be significant since strong screening can reduce V_{pu} by over a factor of 1000 from its value above T_C . This additional capacitive voltage across the pickup coil has a component 90° out of phase from the magnetic part of the pickup voltage. Consider that the phase of I_{dr} in Eq. (1) equals zero, and $\sigma_2 \gg \sigma_1$. A small- C circuit analysis shows that $V_{pu,1} \approx I_{dr} \omega C [M_1/C + R_1 R_2]$ and that $V_{pu,2}$ which without capacitive coupling would be zero is given approximately by

$$|V_{pu,2}| \approx |I_{dr}| \omega^2 C R_1 L_2. \quad (11)$$

Measurements of V_{pu} were made as R_1 was varied, with a thick superconducting Pb foil in place of the film, so that with R_1 near zero, $M_1 = -55$ pH was very small. Note that varying R_1 does not affect the phase of the drive current since R_3 is much greater than the impedance of the coils. Figure 8 shows the out-of-phase pickup voltage, $V_{pu,2}$, increasing linearly with R_1 as predicted. From the slope of the data in Fig. 8 we find that C is roughly 10 pF. By using proper grounding techniques the coupling is generally within 2° of being purely inductive in the “worst case” where

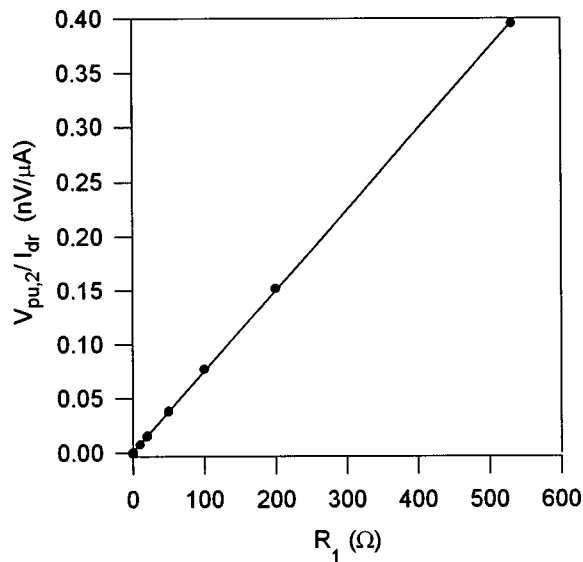


FIG. 8. Data showing the out-of-phase voltage in the pickup coil is linear with the resistance between the drive coil and ground. This extra voltage shows up because of capacitive coupling. A fit to the data combined with a simple model of a single capacitor bridging the drive and pickup coils yields a capacitance, C , of roughly 10 pF. Note that in the experiment R_1 is less than 1 Ω so the capacitive coupling does not affect our measurements significantly.

strong screening is provided by a thick 7.5 mm radius Pb foil at 4 K. When λ is several times larger than the film thickness capacitive coupling ceases to be an issue.

VIII. EFFECT OF HOLES AND DEFECTS

Since the measurement probes a large area of the film, one is concerned about error due to flaws in the films arising from, for example, a small scratch in the substrate that causes a weak section in the film. In an effort to quantify this effect, we measured the mutual inductance when circular Pb foils and Nb films with holes in them were inserted into the apparatus.

First, we looked at holes centered on a 7.5 mm radius, 150 μ m thick Pb foil. For this case, we could also calculate the mutual inductance by setting $\sigma=0$ for ρ less than the radius of the hole. The coils had an experimental *initial position*, $M_E(\infty,0)$, of about 140 nH, and a *zero position*, $M_E(0,0)$ of about -55 pH with a full Pb foil. The negative mutual inductance comes because the drive coil was quadrupolar. The experimental and calculated *zero positions* only differed by 2 pH. (We now achieve much better agreement between calculated and experimental *zero positions* than indicated by Fig. 4 of Ref. 5.) Figure 9 shows the normalized mutual inductance as a function of the radius of the concentric hole. The mutual inductance is essentially equal to the extra coupling through the hole, since the zero position is so small. The calculated curve agrees well with the data. The difference can easily be accounted for by the Pb foil not being exactly concentric with the coils. The measurement becomes sensitive to a centered hole when its radius reaches the radius of the coils.

Next, we looked at Nb films with a hole centered on the most sensitive spot, 1 mm from center, directly underneath

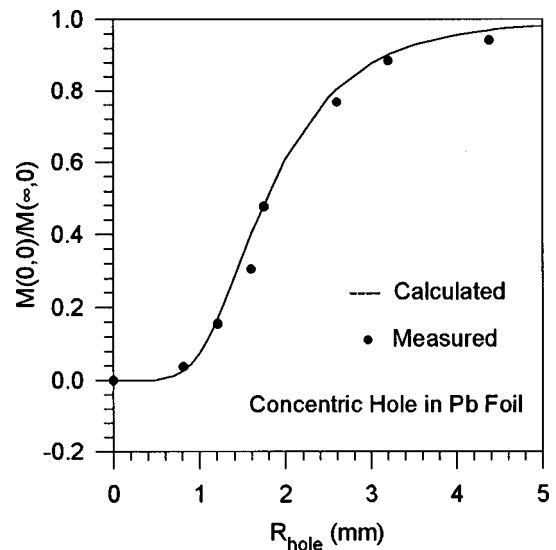


FIG. 9. Normalized mutual inductance with a 15 mm diameter, 150 μ m thick Pb foil screen with a concentric hole cut out placed between the coils. The hole cut out of the center of the Pb has radius, R_{hole} . The dots represent experimental results, and the line is from the numerical calculation for a finite area film.

the windings of the drive coil where the induced current density in the film is largest. The Nb films were e-beam evaporated onto 15 mm diameter circular Si substrates. The mutual inductance was measured as a function of temperature for a number of films. After the initial measurement of $M(T)$, a hole was cut by ion milling the film through a metal mask. The hole diameter ranged from 30 to 600 μ m. T_C was unaffected by the ion milling. For comparison some films were ion milled with a mask without a hole. These films showed no change in $M(T)$. For all films in which a hole was ion milled the mutual inductance increased. The extra mutual inductance is nearly independent of the penetration depth, which changes with T , which indicates that the measured sheet inductance is simply increased by a constant except near T_C , where the effective skin depth of the film approaches $(Rd)^{1/2}$.

Although our modeling cannot calculate directly the effect of holes which are off center, we can get a good estimate by calculating the additional coupling through an annular ring of missing material created by sweeping the hole 360° around the film, then multiplying by the ratio of the area of the hole to the area of the ring.

Figure 10 shows the measured and calculated normalized extra mutual inductance as a function of the hole area, A , for holes centered 1 mm from the center of the film. For holes less than 400 μ m in diameter the extra mutual inductance is nearly proportional to $A^{3/2}$. Figure 11 shows similar data except the size of the hole is fixed (diameter of hole=580 μ m), and the location of the hole is varied. In both cases the agreement with the calculation is excellent. Figure 11 establishes that sensitivity to holes drops off quickly when the hole moves away from the peak in the induced current density.

The quality of the fits enables us to extrapolate to holes much smaller than what we have studied experimentally.

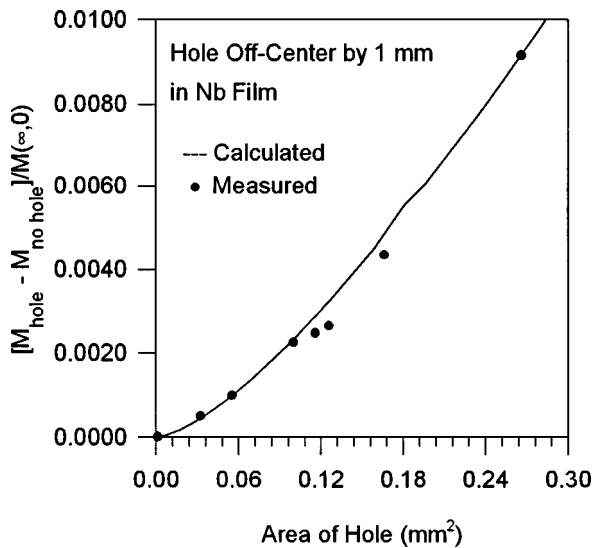


FIG. 10. Extra normalized mutual inductance due to the presence of a hole centered under the drive coil as a function of the hole's area. The dots represent experimental data. The line comes from an approximate solution in which the extra mutual inductance was calculated using the finite radius film routine, Eq. (7), with $\sigma=0$ in an annular ring created by sweeping the hole around the film. This extra mutual inductance was then multiplied by the ratio of the hole's area to the area of the annular ring.

Combining Eq. (6) and Exp. (9), we are led to the following expression in the limit $\sigma_2 \gg \sigma_1$, which is an excellent approximation when λ is not too large, $\lambda/\sinh(d/\lambda) < 20 \mu\text{m}$.

$$\frac{M_E(\lambda, \sigma_1=0) - M_E(0,0)}{M_E(\infty,0)} \approx \frac{\alpha}{M_E(\infty,0)} \frac{\lambda}{\sinh(d/\lambda)}. \quad (12)$$

For our coils, the geometric factor, $\alpha/M(\infty,0)$, is about 2250 m^{-1} . A hole in the film would cause the experimentally determined λ to be larger than the actual value. The thicker the film is the greater the error in λ is for a given hole. For a known λ , the error due to a hole in the film can be calculated from the data in Figs. 10 and 11 combined with Eq. (12). For

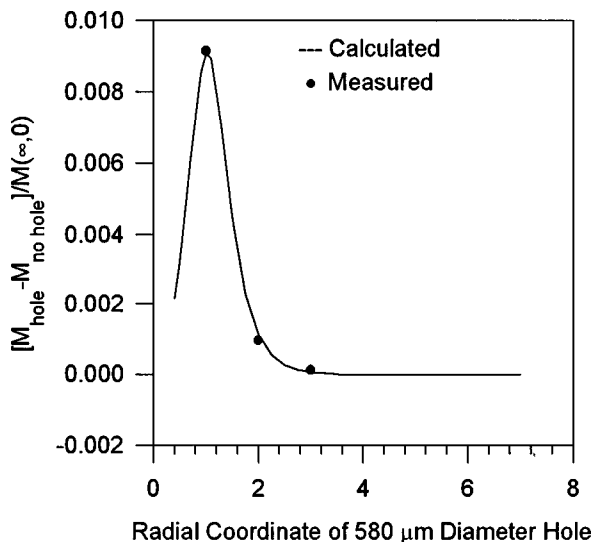


FIG. 11. Extra normalized mutual inductance due to a $580 \mu\text{m}$ diameter hole located at various distances from the center of the film. The line is calculated and the dots are experimental.

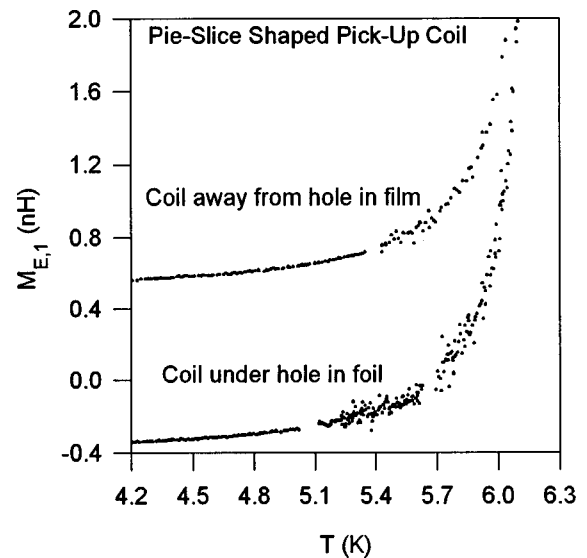


FIG. 12. An example of the mutual inductance using a pie shaped pickup coil of 2 mm radius spanning 60° . The film has a 580 μm diameter hole located 1 mm from the center. A measurement was made with the pie pickup coil located above the hole and a second measurement was made with the pie pickup coil rotated 180° .

a 500 \AA thick film with a penetration depth of 1500 \AA , there is a fair amount of coupling through the film. A $100 \mu\text{m}$ diameter hole located at the center of the film would increase the measured λ by less than 1 \AA . This same hole located directly under the drive coil would increase λ by 40 \AA . Since the extra mutual inductance due to holes is proportional to $A^{3/2}$ it would take 1000 $10 \mu\text{m}$ diameter holes distributed around the film beneath the drive coil to have the same effect as one $100 \mu\text{m}$ diameter hole. Holes up to $600 \mu\text{m}$ in diameter introduce negligible error if they are located 3 mm or further from the center of the film assuming the coils have a 1 mm radius. A $100 \mu\text{m}$ diameter hole in a 5000 \AA thick film located directly under the drive coil would cause a large error, yielding a measured value of $\lambda = 2030 \text{ \AA}$ for an actual penetration depth of 1500 \AA .

To test film homogeneity we use an asymmetric pickup coil which has a pie shape with the vertex beneath the center of the film. The coil spans 60° and has a radial length of 2 mm. For a homogeneous circular film the vector potential will be azimuthal so the only part of the coil which will contribute to the pickup voltage is the circular arc. The two radial portions are perpendicular to the currents and vector potential. Two measurements were made on one of the Nb films with a $580 \mu\text{m}$ diameter hole located at 1 mm. In one case the pie coil was located beneath the hole. For the other measurement the pie coil was rotated 180° . The change in signal was very dramatic. We show the two mutual inductance versus temperature curves in Fig. 12. Because of the hole, the currents are not strictly azimuthal and the radial sections of the pickup coil are contributing to the pickup voltage. Using the pie shaped pickup coils allows one to detect the presence of bad spots or inhomogeneities in a film, even if a hole is not clearly visible. If the $M(T)$ are the same for the pickup coil in different orientations the film is deemed homogeneous on a macroscopic scale and $\lambda(T)$ may

be accurately extracted. However if large differences in $M(T)$ are detected for different orientations of the pickup coil the film has gross inhomogeneities.

IX. CONCLUSION

We have shown how we accurately determine the sheet conductivity of thin films using a two-coil mutual inductance technique and a calculated lookup table. Through detailed comparisons we find that approximating the film as infinite and subtracting from the experimental mutual inductance the mutual inductance going around the film (experimental *zero position*) is an excellent approximation for all experimentally observed conductivities in YBCO for films with radii greater than five times the coil radii. For films of smaller dimension the subtraction procedure yields progressively larger errors and the finite area film calculation with an effective sheet conductivity may be used for the inversion. Using a different coil geometry from the calculations described in the text will change the details of the accuracy of the subtraction procedure. We have also studied the effect of defects on our measurement. Holes 100 μm in diameter and smaller do not introduce a significant error in the measured λ for a 500 \AA thick film, even if they are located directly under the drive coil radius. Even fairly large holes of 500 μm diameter do not have a large effect if they are located sufficiently far from the center of the film. We can conclude that if the film is homogeneous up to three coil radii other than a few de-

fects of length scale less than 100 μm , accurate values of the film conductivity may be obtained even if the outer section of the film has a lot of defects.

ACKNOWLEDGMENTS

The authors thank Rich Kindler, Rita Rokhlin, Tom Kelch, Jay Hunter, Dusan Pejakovic, and Jim Baumgardner for technical assistance. This work was supported by Department of Energy Grant DE-FG02-90 ER45427 through the Midwest Superconductivity Consortium.

- ¹A. F. Hebard and A. T. Fiory, Phys. Rev. Lett. **44**, 291 (1980).
- ²B. Jeanneret, J. L. Gavilano, G. A. Racine, Ch. Leemann, and P. Martinioli, Appl. Phys. Lett. **55**, 27 (1989).
- ³H. Hochmuth and M. Lorenz, Physica C **220**, 209 (1994).
- ⁴Z.-H. Lin, G. C. Spalding, A. M. Goldman, B. F. Bayman, and O. T. Valls, Europhys. Lett. **32**, 573 (1995).
- ⁵S. J. Turneaure, E. R. Ulm, and T. R. Lemberger, J. Appl. Phys. **79**, 4221 (1996).
- ⁶J. Y. Lee, Y. H. Kim, T.-S. Hahn, and S. S. Choi, Appl. Phys. Lett. **69**, 1637 (1996).
- ⁷A. Fuchs, W. Prusseit, P. Berberich, and H. Kinder, Phys. Rev. B **53**, 14 475 (1996).
- ⁸J. H. Claassen, M. L. Wilson, J. M. Byers, and S. Adrian, J. Appl. Phys. **82**, 3028 (1997).
- ⁹J. Gilchrist and E. H. Brandt, Phys. Rev. B **54**, 3530 (1996).
- ¹⁰Th. Klupsch, Physica C **244**, 165 (1995).
- ¹¹A. B. Pippard, Supercond. Sci. Technol. **7**, 696 (1994).
- ¹²J. R. Clem and M. W. Coffey, Phys. Rev. B **46**, 14 662 (1992).